Sensitivity of ray paths to initial conditions

A. Iomin[a] and G.M. Zaslavsky[b,c]

[a] *Department of Physics, Technion, Haifa, 32000, Israel.*

[b] *Courant Institute of Mathematical Sciences,*

New York University, 251 Mercer Str., New York, NY 10012

[c] *Department of Physics, New York University,*

2-4 Washington Place, New York, NY 10003.

Abstract

Using a parabolic equation, we consider ray propagation in a waveguide with the sound speed profile that corresponds to the dynamics of a nonlinear oscillator. An analytical consideration of the dependence of the travel time on the initial conditions is presented. Using an exactly solvable model and the path integral representation of the travel time, we explain the step-like behavior of the travel time T as a function of the starting momentum p_0 (related to the starting ray grazing angle χ_0 by $p_0 = \tan\chi_0$). A periodic perturbation of the waveguide along the range leads to wave and ray chaos. We explain an inhomogeneity of distribution of the chaotic ray travel times, which has obvious maxima. These maxima lead to the clustering of rays and each maximum relates to a ray identifier, *i.e.* to the number of ray semi–cycles along the ray path.

Key words: underwater acoustics, ray chaos, ray travel time

PACS numbers: 05.45.Mt, 05.45.Ac, 43.30.+m, 42.15.-i

INTRODUCTION

The ray tracing has demonstrated that early parts of the time-fronts, *i.e.* ray arrivals in time-depth plane, exhibit surprisingly regular structures simultaneously with sensitivity to the media inhomogeneities that give rise to ray chaos [1–5]. Even at very long ranges, up to a few thousand km, steep chaotic rays can form remarkably stable segments of the time-front, which are very close to their prototypes in the unperturbed waveguide. It turns out that each stable segment in the perturbed waveguide, like its counterpart in the unperturbed one, is formed by rays with equal identifiers, *i.e.* the number of ray semi–cycles.

This phenomenon can be observed in the travel times of the so-called eigenrays, i.e. rays passing through a fixed observation point. In Ref. [6] (see also Refs. [7, 8]) it has been demonstrated that the travel times of chaotic eigenrays usually come in clusters with small time spreads centered at arrivals of unperturbed eigenrays. Although the rays that form a cluster have the same identifier, i.e. the same topology, this does not imply that their trajectories follow close paths. On the contrary, chaotic eigenrays contributing to the given cluster may significantly deviate from each other and from the unperturbed eigenray with the same identifier [3]. These results suggest that while the travel time of chaotic rays is a random function of starting parameters, it is much more predictable as a function of its identifier and the trajectory endpoints, and it also relates to the dependence of the travel time T on the starting momentum p_0 [9]. Interesting, even puzzling features, when observed numerically, reveal a step-like behavior of T as a function of the initial momentum that forms the so-called "shelves" for ray propagation in a range-independent waveguide. In the case when rays propagate in a range-dependent waveguide so-called, ray chaos takes place, and an important characteristic is a ray travel time distribution, which exhibits fairly inhomogeneous features with obvious maxima [9].

In this paper we study analytically the dependence of the travel time on the initial conditions in the framework of an exact solvable model. We consider ray propagation in a waveguide with the sound speed profile which corresponds to the dynamics of a quartic oscillator. Therefore, studying this model, we explain the step-like behavior of the travel time T as a function of the starting momentum p_0 (related to the starting ray grazing angle χ_0 by $p_0 = \tan\chi_0$). For the case when ray chaos takes place due to a range dependent perturbation, we also explain the inhomogeneity of the ray travel time distribution which

has obvious maxima. These maxima lead to the clustering of rays, and each maximum can be related to the corresponding identifier of the cluster of rays.

The paper is organized as follows. In Sec. 2 we give a brief description of ray theory in the small–angle approximation. Explicit expressions for the Hamiltonian determining the ray motion and for the ray travel time are presented. An overview of the numerical results on the ray travel time, obtained in [9], will be presented and explained in the present paper. An exact solution for a simplified speed profile corresponding to the quartic oscillator is considered in Sec. 3. An exact expression for the corresponding classical action as a function of the initial conditions is presented. A detailed analytical analysis of the step-like functional dependence of T on p_0 is performed as well. In Sec. 4 the maxima of the distribution function for the ray travel time are found for the integrable quartic oscillator in the presence of a perturbation. This analysis corresponds to the semiclassical consideration of an amplitude of the wave function in the momentum representation. The conclusion is presented in Sec. 5. Some details of calculations related to the step-function are presented in Appendices A-C.

RAY TRAVEL TIMES

Parabolic equation approximation

Consider a two-dimensional underwater acoustic waveguide with the sound speed c being a function of depth, z, and range, r. The sound wave field u as a function of r, z, and time, t, may be represented as

$$u(r,z,t) = \int d\omega\, \tilde{u}(r,z,\omega)\, e^{-i\omega t}, \tag{1}$$

where the Fourier components $\tilde{u}$ are governed by the Helmholtz equation (see for example[10, 11]):

$$\frac{\partial^2 \tilde{u}}{\partial r^2} + \frac{\partial^2\ \tilde{u}}{\partial z^2} + k^2 n^2 \tilde{u} = 0. \tag{2}$$

Here $k = \omega/c_0$ is a wave number, while $n = c_0/c(r,z)$, is the refractive index and c_0 is a reference sound speed. For the 2D picture, grazing angles are defined as the ratio between the wave numbers k_z and k_r: $\tan\chi = k_z/k_r$, where $k = \sqrt{k_z^2 + k_r^2}$. In the small-angle approximation, when sound waves propagate at small grazing angles with respect to the horizontal, *i.e.* $k_r \approx k$, the Helmholtz equation may be approximated by the standard

parabolic equation [1, 10, 11]. Present $\tilde{u}$ as

$$\tilde{u}(r, z, \omega) = \tilde{v}(r, z, \omega)\, e^{ikr} \tag{3}$$

and substitute this expression into Eq. (2). Taking into account that $\tilde{v}$ is a slowly–varying function of r and neglecting the second derivative of $\tilde{v}$ with respect to r, we derive the parabolic equation

$$2ik\frac{\partial \tilde{v}}{\partial r} + \frac{\partial^2 \tilde{v}}{\partial z^2} + k^2\left(n^2 - 1\right)\tilde{v} = 0. \tag{4}$$

This equation coincides formally with the time-dependent Schrödinger equation. In this case the partial derivative with respect to z is an analog of the momentum operator, *i.e.* $\hat{p} = -ik^{-1}\partial/\partial z$, while r plays the role of time and k^{-1} associates with the Planck constant. In underwater acoustics it is always possible to choose the reference sound speed c_0, such that $|n - 1| \ll 1$, and replace $1 - n^2$ by $2(1 - n) = 2(c(r, z) - c_0)/c_0$.

Since r is a time-like variable, the Hamiltonian system formally coincides with that describing a mechanical particle oscillating in a time-dependent potential well U with the Hamiltonian

$$H = \frac{p^2}{2} + U(z), \tag{5}$$

where

$$U(r, z) = \frac{c(r, z) - c_0}{c_0}. \tag{6}$$

The dimension variable p is an analog to the mechanical momentum. It relates to the ray grazing angle χ by $p = \tan\chi$. The "potential" U in Eq. (6) represents a potential well whose parameters may vary with the range r.

For the point source located at $r = 0$ and $z = z_0$ we have

$$\tilde{v} = \sum_{\nu} A_\nu(z, z_0, r, \omega)\, e^{ikS_\nu(z, z_0, r)}, \tag{7}$$

where the sum goes over contributions from all rays connecting the source and the observation point (r, z). Such rays are called the eigenrays**.** Here $S(z, z_0, r)$ is the eikonal analog to classical action or the Hamilton principal function in mechanics – of the ν-th eigenray. This function is defined by the integral [12]

$$S = \int (pdz - Hdr) \tag{8}$$

over the ray trajectory from $(0, z_0)$ to (r, z).

The amplitude $A(z, z_0, r)$ is given by [13]

$$A = C(\omega) \sqrt{\left| \frac{\partial^2 S}{\partial z \partial z_0} \right|} = C(\omega) \sqrt{\frac{1}{|\partial z / \partial p_0|}}, \tag{9}$$

where $C(\omega)$ is a function determined by the time-dependence of the radiated signal, and the derivative $\partial z / \partial p_0$ is taken at the range r.

Substitution of Eqs. (3) and (7) into Eq. (1) yields

$$u(r, z, t) = \sum_{\nu} \int d\omega \, A_\nu(z, z_0, r, \omega) \, \exp\left(i\omega \left(\frac{r}{c_0} + \frac{1}{c_0} S_\nu(z, z_0, r) - t \right) \right). \tag{10}$$

Each term in this sum represents a sound pulse coming to the observation point through a particular eigenray. The quantity

$$T = \frac{r}{c_0} + \frac{1}{c_0} S(z, z_0, r) \tag{11}$$

determines a delay of the pulse relative to an initially radiated signal and it is called the ray travel time.

Numerical results: an overview of [9]

Studying the general properties of ray travel times in acoustic waveguides is equivalent to studying the properties of the principal Hamiltonian function S of a mechanical particle oscillating in a potential well. Recently the properties of S have been numerically studied in [9]. Hereafter, we refer to this result as SVZ. The main numerical results important for the present analysis are shown in Figs. 1 and 2, which were taken from SVZ. Both figures present the travel time dependence on the starting momentum p_0. Figure 1 demonstrates dependencies of the ray travel time T on the starting momentum p_0 for two waveguides with different sound speed profiles, i.e. for two "potentials" $U(z)$:

$$U_1(z) = az^2 + bz^4, \quad \text{and} \quad U_2(z) = -\gamma z. \tag{12}$$

All six curves shown in Fig. 1 present the travel times at a range of 150 km, and each curve corresponds to a particular source depth. Even though the "potentials" U_1 and U_2 are quite different, both dependencies $T(p_0)$, shown in Figs. 1 and 2, have an important common

feature: each curve has "shelves" where its inclinations with respect to the horizontal are small. At intervals of starting momenta corresponding to the "shelves", the ray travel time T is most stable (least sensitive) with respect to small variations in p_0. The same features occur for the so-called canonical sound speed profile or the Munk profile $c(z) = c_M(z)$, widely used in underwater acoustics to model wave transmission through a deep ocean [10, 14]. The dependencies $T(p_0)$ are shown in Fig. 2 which presents the ray travel times, T, as a function of the starting momentum, p_0, at range of 2500 km for a point source located at 1 km depth. A thick solid line graphs the $T(p_0)$ for the regular ray in the aforementioned range-independent waveguide. Randomly scattered points correspond to chaotic rays in the presence of perturbation: $c(z) = c_M(z) + \delta c(z, r)$. The density of these points has maxima forming dark horizontal stripes, as is shown in Fig. 2. It should be pointed out that, while the background profile $c(z)$ is realistic, the perturbation $\delta c(z, r)$ has been chosen in SVZ to present only a strongly idealized model of internal-wave-induced sound speed variations [15–17]. Nevertheless, this perturbation causes a chaotic ray behavior whose properties closely resemble that observed in more realistic numerical models [1, 2]. Ray travel times in the unperturbed waveguide ($\delta c = 0$) presented in Fig.2 (thick solid line) have the same properties typical of range-independent waveguides, namely "shelves", which are similar to those presented in Fig. 1. Moreover, for the chaotic rays, the stripes of the scattered points are located at travel times close to that of the "shelves" on the unperturbed $T(p_0)$ curves. Note that the unperturbed "shelves" may be interpreted as parts of the $T(p_0)$ curve with the highest density of points depicting unperturbed arrivals. It has been stated in SVZ that, under conditions of ray chaos, the positions of maxima of the density of ray travel times remain relatively stable. So, these figures express the main puzzling results of the generic features of "shelves", and our main task in the present work is to explain them.

A QUARTIC OSCILLATOR

As was mentioned above, the general properties of the ray travel time T can be described by the action S of a mechanical particle in a potential well. Therefore, the generic features of "shelves" for an unperturbed ray can be explained in the framework of an analytical description of the Hamiltonian principal function or the classical action S (8) for an integrable system with some potential U (6). Below we consider the oscillating dynamics of a particle

in the potential U_1 of (12).

Action

As the momentum $p = \tan\chi$ is a dimensionless variable, it is convenient to consider the potential in the dimensionless variables as well. Namely we consider $\sqrt{2a}z \to z$ and $\sqrt{2a}r \to \omega r$, while $b\omega^2/a^2 = \lambda$. Therefore, the dynamical equation for a particle in the potential U_1 (also called a quartic oscillator) in the new notation is

$$\ddot{z} + \omega^2 z + \lambda z^3 = 0. \tag{13}$$

Following to SVZ we take a mass $m = 1$. We also use here, formally, the notation $\ddot{z} \equiv d^2z/dr^2$, *i.e.* the range r plays the same role as a formal time in Hamiltonian dynamics. This equation can be solved exactly. The solution is chosen in the form of the Jacobian elliptic function [18, 19]

$$z(r) = Z\mathrm{cn}\,(\Omega r + \phi_0, \kappa), \tag{14}$$

where Z and ϕ_0 are an amplitude and an initial phase of oscillations correspondingly. The frequency of the nonlinear oscillations is

$$\Omega^2 = \omega^2 + \lambda Z^2 \tag{15}$$

and the modulus of the elliptic functions is

$$2\kappa^2 = \lambda(Z/\Omega)^2. \tag{16}$$

These values are obtained by the straightforward substitution of the solution (14) into (13). Following [19] we take the modulus κ and the initial phase ϕ_0 to be constants of integration. In this case, the solution (14) is

$$z(r) = Z\mathrm{cn}\,(\phi, \kappa) = \left[\frac{2\kappa^2\omega^2}{\lambda(1-2\kappa^2)}\right]^{1/2} \mathrm{cn}\,\left[\frac{\omega r}{\sqrt{1-2\kappa^2}} + \phi_0, \kappa\right], \tag{17}$$

where κ and ϕ_0 are associated with the initial coordinate z_0 and momentum p_0 as

$$z_0 = z(r=0) = Z\mathrm{cn}\,(\phi_0, \kappa), \quad p_0 = \dot{z}(r=0) = -Z\Omega\mathrm{sn}\,(\phi_0, \kappa)\mathrm{dn}\,(\phi_0, \kappa) \tag{18}$$

with sn and dn are also Jacobian elliptic functions. It is simple to see from (18) that κ is the integral of motion related to the Hamiltonian

$$\kappa = \sqrt{\lambda H/\omega^4}, \tag{19}$$

while the initial phase is

$$\phi_0 = \mathrm{cn}^{-1}[\omega z/\sqrt{2H}]. \tag{20}$$

It also follows from (18) that for $p_0 > 0$, the initial phase changes in the range $3K(\kappa) < \phi_0 < 4K(\kappa)$ (or $-K(\kappa) < \phi_0 < 0$), where $K(\kappa)$ is the elliptic integral of the first kind. The modulus is restricted by $0 \leq \kappa^2 < 0.5$, and the relations between the constants of integration and the initial conditions are expressed by the single–valued functions.

Inserting (17) in (8), and using the integrals (312.02), (312.04), (361.02) of the Ref. [18] and the formulas for the elliptic integral of the second kind [19]

$$E(\phi) - E(\phi') = E(\phi - \phi') - \kappa^2 \mathrm{sn}\,(\phi)\mathrm{sn}\,(\phi')\mathrm{sn}\,(\phi - \phi'),$$

we obtain the following expression for the action S

$$S = \frac{-2\omega^2\Omega}{3\lambda}E(\Omega r) + \Omega^4 r(1-\kappa^2)(2-3\kappa^2)/3\lambda + \frac{2\omega^2\Omega\kappa^2}{3\lambda} \times$$
$$\left\{\mathrm{sn}\,(\phi_0)\mathrm{sn}\,(\phi)\mathrm{sn}\,(\Omega r) + \frac{\Omega^2}{\omega^2}[\mathrm{sn}\,(\phi_0)\mathrm{cn}\,(\phi_0)\mathrm{dn}\,(\phi_0) - \mathrm{sn}\,(\phi)\mathrm{cn}\,(\phi)\mathrm{dn}\,(\phi)]\right\} \tag{21}$$

where

$$\phi = \Omega r + \phi_0, \quad \Omega = \frac{\omega}{\sqrt{1-2\kappa^2}}.$$

The following notations $E(x) \equiv E(x,\kappa)$ and $\mathrm{sn}\,(x) \equiv \mathrm{sn}\,(x,\kappa)$ (the same for $\mathrm{cn}\,, \mathrm{dn}\,$) are used.

"Shelves" in the small κ approximation

The small κ approximation. The expression for the action S can be simplified. Since $\kappa^2 < 0.5$, one can use the small–κ–approximation for the elliptic integrals. Using the following definition for the elliptic integral [21]

$$E(x,\kappa) \equiv E(x) = x - \kappa^2 \int_0^x \mathrm{sn}\,(x')dx'$$

and the approximation $\mathrm{sn}\,(x) \approx \sin(x)$, we obtain approximately that

$$E(x) \approx x - x\kappa^2/2 - \kappa^2 \sin(2x)/4. \tag{22}$$

Inserting(22) in (21), and then combining the first two terms, we obtain, after doing small algebra, the following expression for the action

$$S(\kappa) \approx \frac{\omega^4 r\kappa^4}{3\lambda} - \frac{\omega^3\kappa^2}{2\lambda}\left[\sin(2\phi) - \sin(2\phi_0)\right], \tag{23}$$

where the nonlinear frequency is now $\Omega \approx \omega(1+\kappa^2)$. It also follows in this approximation that the relation (18) between the initial momentum p_0 and the modulus κ is simplified

$$p_0 \approx g\kappa, \tag{24}$$

where $g = -\omega\sqrt{2/\lambda}\sin\phi_0$, and $-\pi/2 \leq \phi_0 < 0$. The dependence of ray travel times on the initial momentum $T(p_0)$ in SVZ coincides up to some constant multiplier with the dependence of the action on the modulus $S(\kappa)$ in (23).

"Shelves." It follows that the action in the form (23) consists of two terms. The first one is the dominant (proportional to $\omega r \gg 1$) monotonic growing function in κ. The second one is the small but fast oscillating term with a large frequency (proportional to $\omega r \gg 1$). Such a combination of these two terms ensures the monotonic growth of the function in general, but at the same time the extrema equation $\partial S/\partial\kappa = 0$ has solutions. These solutions can be simply obtained, *e.g.* for $\phi_0 = 0$. The extremum points condition gives, in the same limit $\omega r \gg 1$, the following solutions for κ

$$2\phi = 2\Omega(\kappa)r + 2\phi_0 = \pm\arccos(2/3) + 2\pi m + O(1/\omega r) \equiv \phi_m^{\pm}, \tag{25}$$

where $m > \omega r/\pi$ are integer numbers and $O(1/\omega r)$ means neglected terms of the order of $1/\omega r \ll 1$.

Therefore, there are regions between extrema points (ϕ_m^-, ϕ_m^+) with the same number m where the derivatives are negative, $\partial S/\partial\kappa < 0$. It follows that, in a range of $\Delta\kappa = \Delta_- \approx \pi/8\omega r\kappa$, the action S decreases by ΔS_- (see Appendix A). These regions alternate with regions of growth, where $\partial S/\partial\kappa > 0$. Between extremum points (ϕ_m^+, ϕ_{m+1}^-) on the range of $\Delta\kappa = \Delta_+ = 3\Delta_-$ the action changes as

$$\Delta S_+ = 9\Delta S_- \tag{26}$$

Therefore the growth of the action is stronger (by 9 times) than the decrease that leads to the step-like behavior of the action as a function of κ. This step–like function (see Figs. 1 and 3) has horizontal parts called "shelves" in [9].

An important feature of "shelves" is a large number of Fourier components in the Fourier transformation of the oscillating term in (23) (see Appendix B). It is shown in Appendix C that the average number of "harmonics" of the Fourier transformation is

$$\langle D_s \rangle \approx \omega r \gg 1 \tag{27}$$

One can see, in the insert of Fig. 3, a large number of the Fourier amplitudes.

TRAVEL TIME DISTRIBUTION FOR CHAOTIC RAYS

In contrast to the regular dynamics, the arrival times of chaotic rays are not uniquely defined functions of the initial conditions, which is a simple result of the energy H (5) or the modulus κ being no more the integrals of motion in the chaotic case. This means that many initial conditions can contribute to the same arrival time (as it is seen in Fig. 2). Wave dynamics leads to the wave superposition with different probabilities for different arrival times. Obvious maxima of the travel times distribution are seen in Fig. 2. To explain this phenomenon, we will use the analytical solution for the unperturbed ray dynamics, while chaotic dynamics is modeled by a randomization of the initial phase ϕ_0 or by a variety of different sources with random phases ϕ_0 uniformly distributed in the interval $(-\pi/2, 0)$.

An integrable case. The probability of finding a particle with the range r and the depth z is defined by a solution of the parabolic equation (4) with an amplitude (9). Therefore these amplitudes define the probability distribution for different $S(\kappa)$ with the same fixed r by (9)

$$|A(r,z)|^2 \propto |\partial z/\partial p_0|^{-1}. \tag{28}$$

Taking into account the solution $z(r)$ in (17) and the relation $p_0(\kappa)$ in (24), we obtain in the small–κ–approximation

$$\begin{aligned} \partial z/\partial p_0 &= (\partial\kappa/\partial p_0)\cdot(\partial z/\partial\kappa) + (\partial\phi_0/\partial p_0)\cdot(\partial z/\partial\phi_0) \\ &\approx [4\omega r\kappa^2\cos\phi_0\sin\phi - 2\cos(\phi+\phi_0)]/\sin(2\phi_0) \end{aligned} \tag{29}$$

In the limit $\omega r \gg 1$, the main contribution to the derivative (29) is due to the linear term $\phi \sim \omega r$. Therefore the evaluation of the probability for the asymptotically large times is

$$|A|^2 \approx \frac{1}{2\omega r\kappa^2}\left|\frac{\sin(\phi_0)}{\sin\phi}\right|. \tag{30}$$

The maxima of this probability correspond to zeroes of the denominator, which can be found from the following equation

$$\phi(\kappa=\kappa_n) = \phi_0 + \Omega(\kappa_n)r = \phi_0 + \omega r(1+\kappa_n^2) = \pi n, \qquad n = 0,1,2,\ldots \tag{31}$$

For the fixed ωr and ϕ_0, the solutions of (31) $\kappa = \kappa_n$ determine the actions $S_n = S(\kappa_n)$ where the maxima of probability take place for the integrable case.

Ray chaos. For the chaotic case the energy H or the modulus κ are no longer the integrals of motion. Therefore the rays with different initial conditions κ, ϕ_0 can contribute to the same arrival time S with different probabilities. In our phenomenological approach, it is convenient, as was mentioned above, to model the chaotic dynamics by a variety of initial conditions with random phases ϕ_0 uniformly distributed in the interval $(-\pi/2, 0)$. Therefore the averaged probability is a superposition of probabilities with all initial phases. It reads

$$\langle |A|^2 \rangle = \frac{2}{\pi} \int_{-\pi/2}^{0} |A|^2 d\phi_0 = \frac{\pm 1}{\omega r \kappa^2} \left(\sin(\Omega r)/8 - (1/\pi) \cos(\Omega r) \ln \left[-\tan(\Omega r) \right] \right), \qquad (32)$$

where the signs $\pm$ are due to the modulus function in (30) and (32), and $(+)$ sign stands for $-\pi/2 < (\Omega r, \mod 2\pi) < 0$, while $(-)$ sign is taken for $\pi/2 < (\Omega r, \mod 2\pi) < \pi$. The maxima of the mean probability are

$$\Omega(\kappa_n) r = \omega r (1 + \kappa_n^2) = \pi n, \qquad (33)$$

that coincides with (31) for $\phi_0 = 0$. It follows from (31) and (32) that rays with different κ are clustered by the index n numbering the maxima. For all values of ϕ_0 one always finds a value of κ which corresponds to the maxima conditions with the same n. It also follows that all other values of κ which do not correspond to the maxima conditions "carry" the same index n if their action S is close to the maximum value $S(\kappa_n)$. This phenomenon of the ray clustering can be a possible explanation of the *ID number* for rays [9].

CONCLUSION.

It should be admitted that in the framework of this simple analysis of the solution of the quartic oscillator, we are able to describe fairly well the step–like behaviour of the arrival paths as a function of the initial momentum. This step–like behaviour is known as "shelves" [9].

For the chaotic behaviour of rays, we constructed a phenomenological model and presented only qualitative explanations of the nonuniform distribution of the arrival paths as a function of the initial momentum. The maxima of this distribution are explained in the framework of the integrable model. Such a kind of consideration corresponds to a so–called linear response approximation.

This work was supported by the U.S. Navy Grant N00014-97-1-0426. We thank A. Pitt for her help in preparing this paper.

Appendix A

The extremum points condition gives in the same limit $\omega r \gg 1$ the following solutions for κ

$$2\phi = 2\Omega(\kappa)r + 2\phi_0 = \pm \arccos(2/3) + 2\pi m \equiv \phi_m^{\pm}, \tag{A. 1}$$

where $m > \omega r/\pi$ are integers numbers. The phases ϕ_m^+ stand for the minima of S with

$$\partial^2 S(\phi_m^+/\partial\kappa^2 \equiv S''_{m,+} = 8\sqrt{5}\omega^5\kappa^4 r^2 > 0, \tag{A. 2}$$

while ϕ_m^- define the maxima of the action,

$$\partial^2 S(\phi_m^-/\partial\kappa^2 \equiv S''_{m,-} = -8\sqrt{5}\omega^5\kappa^4 r^2. \tag{A. 3}$$

It is simple to see that the regions on κ between any adjoint extrema are very small. Indeed, the width of the region where the action decreases, Δ_- is determined from (25)

$$\phi_m^+ - \phi_m^- = 2\omega r[(\kappa + \Delta_-)^2 - \kappa^2] = \pi/2,$$

where we took approximately that $\arccos(2/3) \approx \pm\pi/4$. From where we obtain that

$$\Delta_- \approx \pi/8\omega r\kappa. \tag{A. 4}$$

Analogously, from $\phi_{m+1}^- - \phi_m^+ = 3\pi/2$ we obtain that the width of the region where S increases is

$$\Delta_+ = 3\Delta_-. \tag{A. 5}$$

Since $\Delta_\pm \ll 1$, we can define both a growth ΔS_+ and a decrease ΔS_- of the action in corresponding regions between adjoined extremal points in the linear approximation. Expanding the first derivative $\partial S/\partial\kappa$ near every extremal point, we obtain for ΔS_-

$$\Delta S_- = \int_0^{\Delta_-/2} S''_{m,-} x dx + \int_0^{\Delta_-/2} S''_{m,+}(-x) dx.$$

Inserting (A. 2) and (A. 4) in the integration, we obtain that

$$\Delta S_- = -\pi^2\sqrt{5}\omega^3\kappa^2/16. \tag{A. 6}$$

Carrying out the same for ΔS_+ we obtain

$$\Delta S_+ = 9|\Delta S_-|. \tag{A. 7}$$

Appendix B

Let us rewrite the oscillating term in the form

$$\sin(2\phi) = \sin(2\omega r + 2\phi_0)\cos(\omega r\kappa^2) + \cos(2\omega r + 2\phi_0)\sin(\omega r\kappa^2). \quad \text{(B. 1)}$$

For simplicity we consider $\kappa \in [0,1]$ by rescaling $2\kappa^2 \to \kappa^2$ that does not lead to any errors in the analysis. Since the region of definition of $\sin(2\phi)$ is restricted by this segment, it is not difficult to show that the coefficients of the Fourier transformation $f^C(s), f^S(s)$ are determined by the Fresnel integrals $C(s), S(s)$ [20, 21]:

$$f^C(s) = \int_0^1 d\kappa \sin(2\phi)\cos(2\pi s\kappa), \quad f^S(s) = \int_0^1 d\kappa \sin(2\phi)\sin(2\pi s\kappa). \quad \text{(B. 2)}$$

Carrying out the variable change $x = \omega r\kappa$ and considering that $\omega r \gg 1$ we take the upper limit to ∞. Then we have for (B. 2) the following four integrals which determine the coefficients $f^C(s), f^S(s)$

$$\int_0^1 d\kappa \sin(\omega r\kappa^2)\sin(s\kappa) \to \frac{1}{\sqrt{\omega r}} \int_0^\infty dx \sin(x^2/\omega r)\sin(\frac{s}{\omega r}x)$$

and it gives

$$\sqrt{\frac{\pi}{2\omega r}} \left\{ \cos\frac{s^2}{4\omega r} C\left(\frac{s}{2\sqrt{\omega r}}\right) + \sin\frac{s^2}{4\omega r} S\left(\frac{s}{2\sqrt{\omega r}}\right) \right\},$$

Analogously we obtain for the rest of integrals

$$\int_0^1 d\kappa \sin(\omega r\kappa^2)\cos(s\kappa) \approx \sqrt{\frac{\pi}{8\omega r}} \left\{ \cos\frac{s^2}{4\omega r} - \sin\frac{s^2}{4\omega r} \right\},$$

$$\int_0^1 d\kappa \cos(\omega r\kappa^2)\cos(s\kappa) \approx \sqrt{\frac{\pi}{8\omega r}} \left\{ \cos\frac{s^2}{4\omega r} + \sin\frac{s^2}{4\omega r} \right\},$$

$$\int_0^1 d\kappa \cos(\omega r\kappa^2)\sin(s\kappa)$$

$$\approx \sqrt{\frac{\pi}{2\omega r}} \left\{ \sin\frac{s^2}{4\omega r} C\left(\frac{s}{2\sqrt{\omega r}}\right) - \cos\frac{s^2}{4\omega r} S\left(\frac{s}{2\sqrt{\omega r}}\right) \right\}.$$

Keeping $\Delta s \Delta x > const$, we obtain that there are of the order of $\omega r \gg 1$ components with the amplitudes $\sim 1/\sqrt{\omega r}$ contributed to the Fourier transformation.

Appendix C

The oscillating part of the action S has a complete oscillation between points $(\phi_m^{\pm}, \phi_{m+1}^{\pm})$ that corresponds to the range on κ or a quasi–period equaled to

$$D_\kappa = \Delta_+ + \Delta_- = 4\Delta_-. \tag{C. 1}$$

Hence, taking into account (A. 4), we obtain that the number of harmonics in the Fourier transformation is

$$D_s = 2\pi/D_\kappa = 4\omega r\kappa. \tag{C. 2}$$

Since $0 < \kappa^2 < 0.5$, the averaging of (C. 2) gives

$$\langle D_s \rangle = \omega r. \tag{C. 3}$$

It should be stressed that this estimate is approximate and gives only the order of D_s. The exact theorem on the uncertainty conditions (see for example [22]) ensures only that $\langle D_s \rangle > \omega r/\sqrt{8\pi}$.

[1] J. Simmen, S.M. Flatte, and G.-Y. Wan, Wavefront folding, chaos, and diffraction for sound propagation through ocean internal waves, J. Acoust. Soc. Am. 102 (1997) 239–255.

[2] M.G. Brown and J. Viechnicki, Stochastic ray theory for long-range sound propagation in deep ocean environment, J. Acoust. Soc. Am. 104 (1998) 2090–2104.

[3] F.J. Beron-Vera, M.G. Brown, J.A. Colosi, S. Tomsovic, A.L. Virovlyansky, M.A. Wolfson, and G.M. Zaslavsky, Ray dynamics in the AET experiment, unpublished.

[4] P. F. Worcester, B. D. Cornuelle, M. A. Dzieciuch, W. H. Munk, M. Howe, A. Mercer, R. C. Spindel, J. A. Colosi, Metzger, T. Birdsall, and A. B. Baggeroer, A test of basin-scale acoustic thermometry using a large- aperture vertical array at 3250-km range in the eastern north pacific ocean, J. Acoust. Soc. Am. 105 (1999) 3185–3201.

[5] J. A. Colosi, E. K. Scheer, S. M. Flatte, B. D. Cornuelle, M. A. Dzieciuch, W. H. Munk, P. F. Worcester, B. M. Howe, J. A. Mercer, R. C. Spindel, K. Metzger, T. Birdsall, and A. B. Baggeroer, Comparisons of measured and predicted acoustic fluctuations for a 3250-km propagation experiment in the eastern north pacific ocean, J. Acoust. Soc. Am. 105 (1999) 3202–3218.

[6] F.D. Tappert and X. Tang, Ray chaos and eigenrays, J. Acoust. Soc. Am. 99 91996) 185–195.

[7] D.R. Palmer, T.M. Georges, and R.M. Jones, Classical chaos and the sensitivity of the acoustic field to small-scale ocean structure, Comput. Phys. Commun. 65 (1991) 219–223.

[8] J.L. Spiesberger and F.D. Tappert, Kaneohe acoustic thermometer further validated with rays over 3700 km and the demise of the idea of axially trapped energywavefront folding, chaos, and diffraction for sound propagation through ocean internal waves, J. Acoust. Soc. Am. 99 (1996) 173–184.

[9] I.P. Smirnov, A.L. Virovlyansky, and G.M. Zaslavsky, Sensitivity of ray travel times, Chaos 12 (2002) 617–635.

[10] L.M. Brekhovskikh and Yu. Lysanov, Fundamentals of Ocean Acoustics, Springer-Verlag, Berlin, 1991.

[11] F.B. Jensen, W.A. Kuperman, M.B. Porter, and H. Schmidt, Computational Ocean Acoustics, AIP, Woodbury, New York, 1994.

[12] L.D. Landau and E.M. Lifshitz, Mechanics, third ed., Pergamon Press, Oxford, 1976.

[13] M.C. Gutzwiller, Phase-integral approximation in momentum space and the bound states of an atom, J. Math. Phys. 8 (1967) 1979–2000.

[14] S.M. Flatte, R. Dashen, W.M. Munk, K.M. Watson, and F. Zakhariasen, Sound transmission through a fluctuating ocean, Cambringe U.P., London, 1979.

[15] K.B. Smith, M.G. Brown, and F.D. Tapper, Ray chaos in underwater acoustics, J. Acoust. Soc. Am. 91 (1992) 1939–1949.

[16] G.M. Zaslavsky and S.S. Abdullaev, Chaotic transmission of waves and "cooling" of signals, Chaos 7 (1997) 182–186.

[17] I.P. Smirnov, A.L. Virovlyansky, and G.M. Zaslavsky, Theory and applications of ray chaos to underwater acoustics, Phys. Rev. E 64 (2001) 036221.

[18] P.F. Byrd and M.D. Friedman, Handbook of Elliptic Integrals for Engineers and Scientists, Springer-Verlag, Berlin, 1971.

[19] M.M. Mizrahi, The semiclassical expansion of the anharmonic–oscillator propagator," J. Math. Phys. 20 (1979) 845–855.

[20] I.S. Gradshteyn and I.M. Ryzhik, Table of Integrals Series and Products, Academic Press, New York, 1965.

[21] M. Abramowitz and I.A. Stegun, Handbook of Mathematical Functions, Washington, 1968.

[22] A. Papoulis, The Fourier integral and its applications, McGraw–Hill, New York, 1962.

Figure captions

Fig. 1. The ray travel time as a function of starting momentum for two waveguides with the sound speed profiles $c_1(z) = c_{01} + az^2 + bz^4$ (curves a, b, and c), and $c_2(z) = c_{02} - \gamma z$ (curves d, e, and f). Parameters: $c_{01} = 1.49$ km s^{-1}, $a = 1.$ km^{-1}s^{-1}, $b = 1.$ km^{-3} s^{-1}, $c_{02} = 1.4465$ km s^{-1}, $\gamma = 0.0435$ s^{-1}. It has been assumed that the waveguide with $c_1(z)$ has no boundaries, while $c_2(z)$ has a reflecting surface at $z = 0$. The travel time at each curve is estimated from the arrival of the ray with $p_0 = 0$. Different curves present rays escaping point sources located at depths: 0 km (a), 0.5 km (b), 1 km (c), 0 km (d), 1 km (e), and 2 km (f). [from Ref. [9]]

Fig. 2. The ray travel time versus starting momentum in the unperturbed (thick solid lines) and perturbed (points) waveguides at the range of 4500 km and for the point source set at a depth of 2.5 km. [from Ref. [9]]

Fig. 3. The ray travel time (action S versus the modulus κ for Eq. (23), where $\phi_0 = -\pi/4,\ \omega = 1,\ r = 355.4,\ \lambda = 1.2$. The insert is the amplitudes $f(s)$ vs s of the discrete Fourier transformation for the oscillating part of the action S (B. 2).

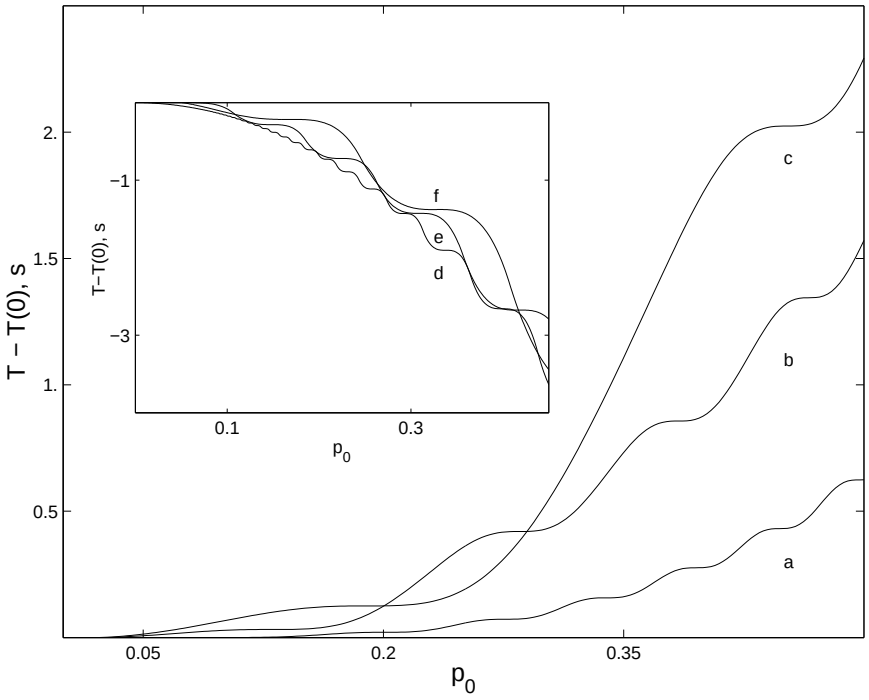

Figure 1:

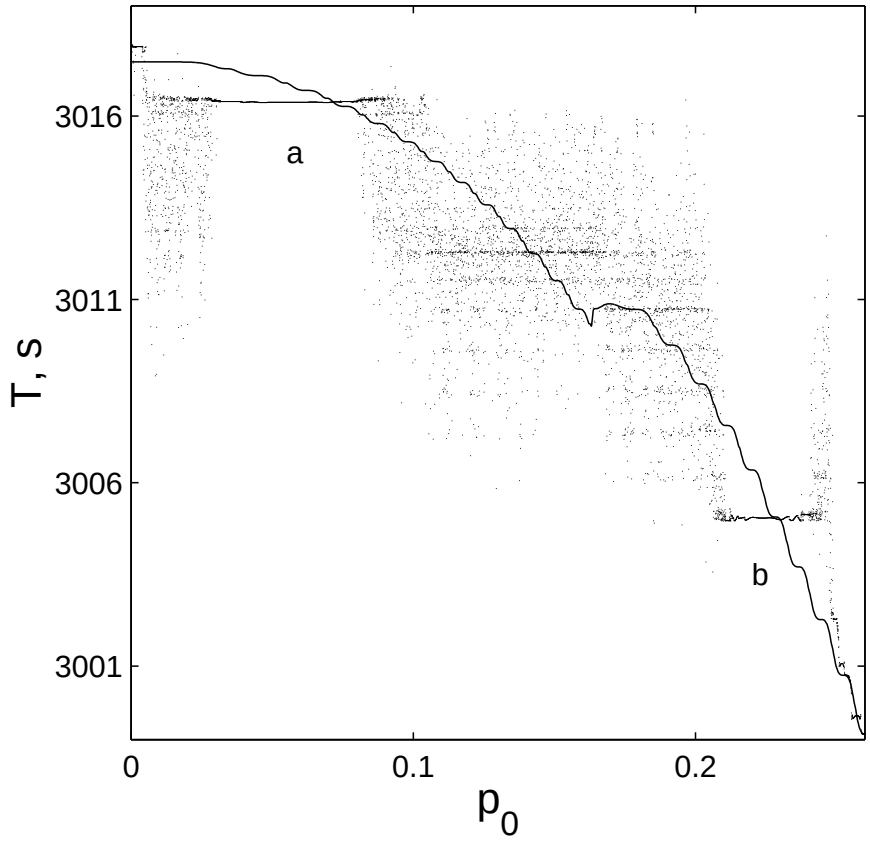

Figure 2:

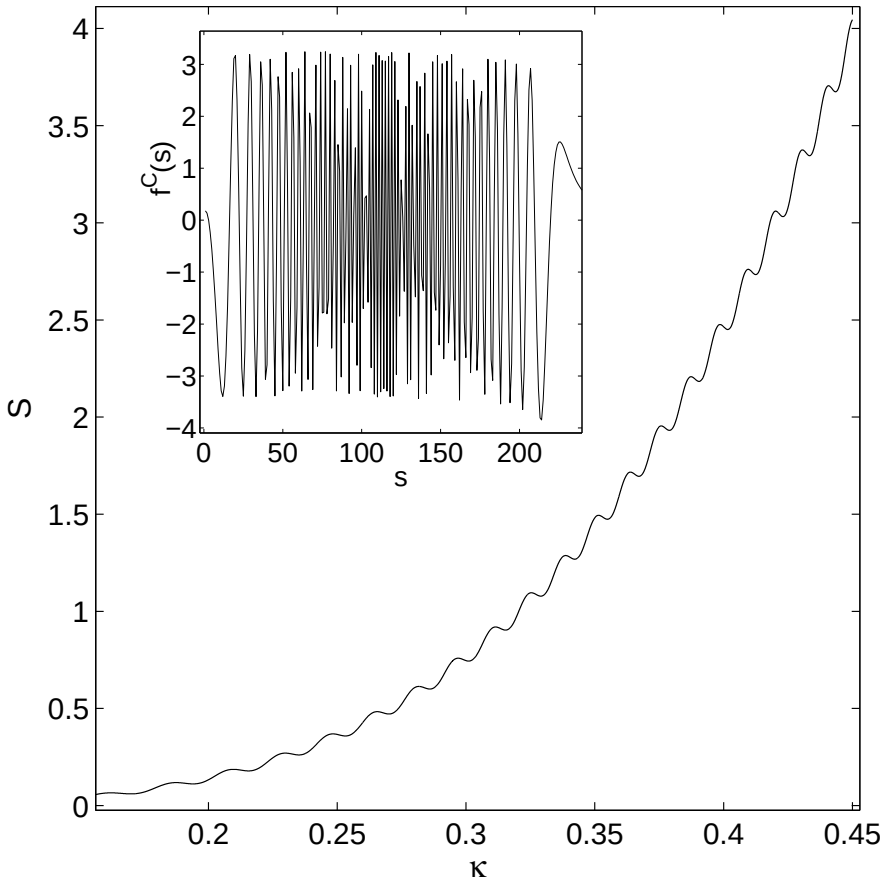

Figure 3: